Supporting Information

Gaglia et al. 10.1073/pnas.1311126110

Mathematical Modeling and Parameter Search

The model for p53 oligomerization consists of three ordinary differential equations (Table S1), with eight parameters listed in Table S2. Because of the lack of experimental techniques capable of measuring tetramerization in vivo, most of the parameters of the model are not available in the literature. Table S3 includes a list of relevant biophysical measurements available in the literature or measured in this work.

Our goal is to identify a global pattern of behavior independent of parameter sets. The model is therefore nondimensional, meaning that the variables and the parameter values are unitless. Comparison of model parameters to known experimental values (Table S3) would require defining scales for concentration and time, arbitrarily chosen and potentially misleading. Furthermore, a fitting procedure could have provided us with the parameter sets that best described the data. However, we decided against fitting our model to the data because the degrees of freedom of the parameters outweighed the constraints our data could pose on them. This will result in multiple solutions for the parameter space without a clear way of testing which solution would be more appropriate.

Instead we kept the values of each parameter equal to a power of 10—that is, having every step change in parameter correspond to one order of magnitude. We then used the data collected from the fluorescence correlation spectroscopy (FCS) measurement on the cell line expressing p53wt-mCerulean before stress as described below:

a) we first allowed each parameter to attain the each of seven possible parameter values, 10^i, where $i = -3, -2, -1, 0, +1, +2, +3$, spanning seven orders of magnitude; this created a combinatorial set of over 5 million possible parameter sets;

b) we derived analytically the steady-state solutions of the ODEs (ordinary differential equations) in Table S1, and we calculated the steady-state values for the three species of p53 for each parameter set; and

c) we narrowed down the plausible parameters sets using three measurements:

i) the brightness of wild-type p53 at time 0, from Fig. 1*C*, +/− 5%,

ii) the dimer/monomers and tetramers/monomers ratios, from Fig. 1*D*, +/− 50%, and

iii) requiring that $b_t > b_d > b_m$ from Fig. 2.

Using these criteria we narrowed down the parameter space to 349 sets. Fig. S3 shows that a combined effect, of both degradation decrease and oligomerization increase, is required to match the trend in the experimental evidence (Fig. 3*E*) independent of parameter values.

To model the perturbations caused by DNA damage, we modified the corresponding parameters b_m, b_d, and b_t for changes in degradation and k_{on}^{tet} and k_{off}^{tet} for changes in the tetramerization reaction. We attempted both step changes, linear and exponential decays for both reduction in degradation and the stabilization of tetramerization. Qualitatively the main conclusion from the model holds true under all types of perturbations of the model we tested, clearly with quantitative differences in overall timescale of simulation and magnitude of total p53 increase (in fact, as Fig. S3 shows, even with the same type of perturbation, different parameter sets have faster dynamics than others). For Fig. 3 and Fig. S3, the degradation decay is simulated as an exponential decay. The degradation rates of all three species of p53 (monomeric, dimeric, and tetrameric) were lowered by the same proportion, hence keeping the ratios between degradation constants the same as before damage. The stabilization of tetramerization is modeled as a linear decrease in tetramerization off-rate and linear increase in tetramerization on-rate.

SI Materials and Methods: FCS Brightness Validation Measurement in Cell Lysate

The acquired plasmid promoterless monomeric teal fluorescent protein (pmTFP) was cut out and inserted into an enhanced yellow fluorescent protein (EYFP)–C1 vector by NheI/BglII to form pmTFP–C1 vector. Tandem TFP–TFP plasmid was generated by inserting a TFP ORF generated by PCR into the pmTFP–C1 vector by Sal1/Mfe1 into Xho1/Mfe1. 293T (human embryonic kidney) cells were seeded into a 10-cm Petri dish, and antibiotics were removed 1 d before the transfection. Transient transfection of TFP and TFP–TFP plasmid into 293T cell was carried out using Lipofectamine LTX and PLUS reagents (Invitrogen). Total 10 μg DNA plasmid was added with Opti-MEM media with Lipofectamine LTX and PLUS to cells at 50% confluence. Cells were harvested 1 d after transfection, pelleted, and resuspended in 100 μL lysate buffer (20 mM Hepes, 5 mM KCl, 1.5 mM MgCl2, and protease inhibitors; Roche). The lysate was incubated on ice for 30 min followed by centrifugation at 16,000 × *g* at 4 °C for 30 min. The supernatant was further centrifuged at 110,987 × *g* at 4 °C for 30 min. The collected supernatant was diluted in lysate buffer for FCS measurement. The laser power was set to 10 mw, a level at which no photobleaching was observed.

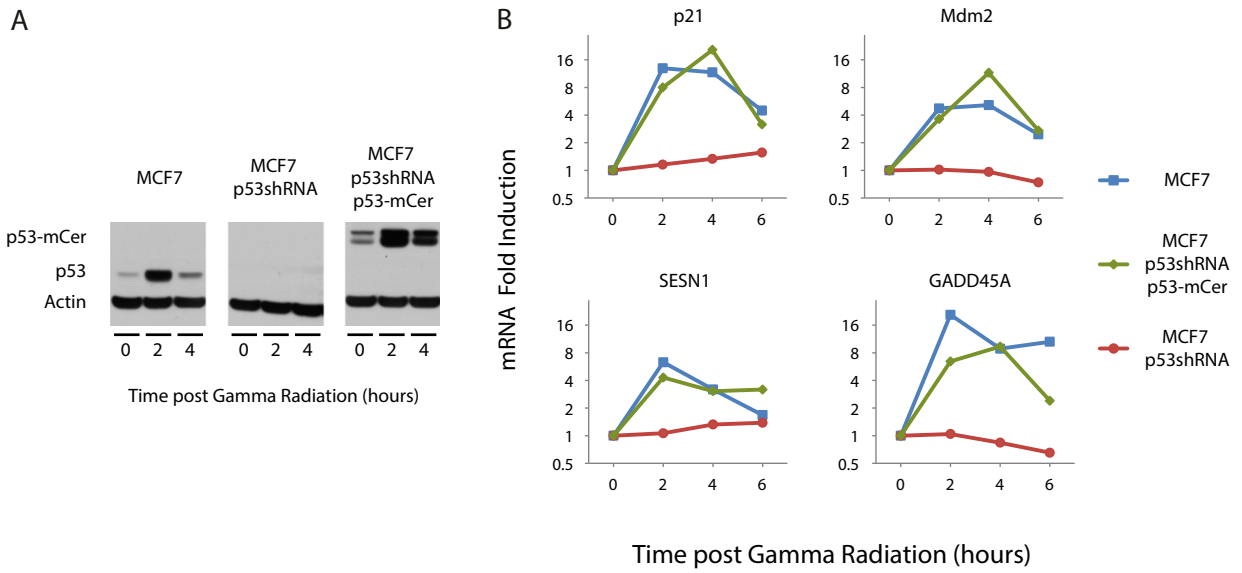

Fig. S1. (*A* and *B*) C-terminal tagging of p53 with mCerulean does not disrupt the dynamics and function of p53. (*A*) p53 levels were measured using immunoblots in parental MCF7 cells, MCF7 cells silenced for p53 (p53 shRNA), and cells expressing p53 tagged to mCerulean. (*B*) mRNA levels of p53 target genes measured using qPCR. The reintroduced tagged p53–mCerulean is able to induce expression of p53 target genes.

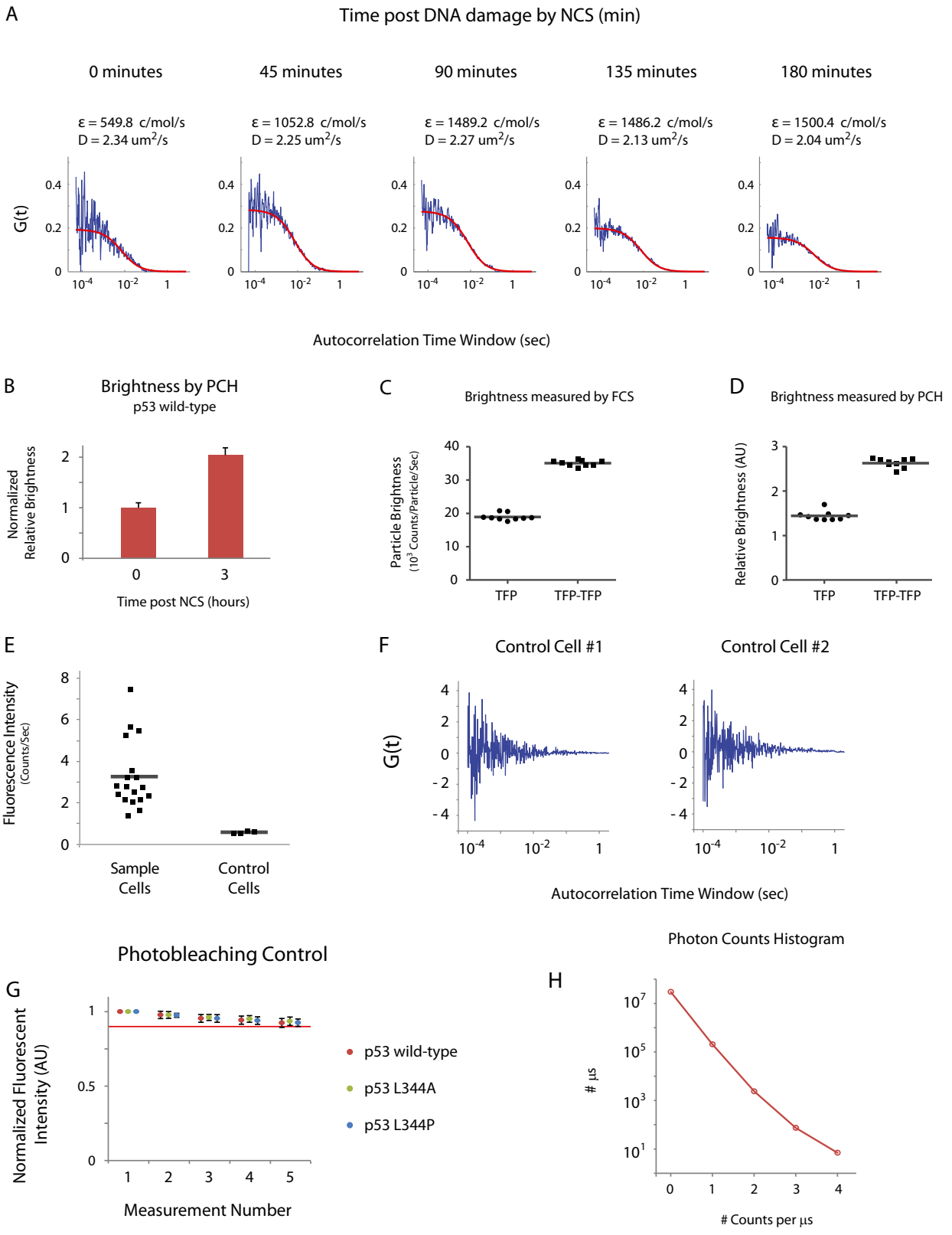

Fig. S2. (*A*) An example for FCS autocorrelation traces and fits in one cell. Autocorrelation G(t) is calculated by averaging five 30-s measurements at a specific time point after DNA damage. The autocorrelations were fit to theoretical curves assuming Brownian diffusion (red line). The values for the diffusion constant D and brightness ε for the correspondent traces are calculated by the fitting of the autocorrelation curves. (*B*) The relative brightness of wild-type p53 calculated by photon counting histogram (PCH) technique at rest and 3 h after DNA damage (mean +/− SEM, $n = 5$) shows the same behavior as the molecular brightness calculated by FCS (WT in Fig. 1C). (*C* and *D*) Particle brightness of single TFP and tandem dimer TFP in cell lysates measured by FCS and PCH. Each dot corresponds to a fluorescent measurement, and the gray line is the sample average. (*E*) Comparison of fluorescence intensity of sample cells expressing

Legend continued on following page

p53-mCerulean and control cells not expressing the fluorescent reporter (gray line represents the sample average). (*F*) FCS analysis of two control cells not expressing the fluorescent reporter. The background signal does not show any autocorrelation. (*G*) Photobleaching was minimal for all of the cell lines used, expressing either p53 wild-type or p53 mutants L344A and L344P, in five consecutive measurements (mean and SD, $n = 25$ for p53 wild type, $n = 20$ for p53 L344A, and $n = 15$ for p53 L344P). The red line represents the 0.9 intensity normalized by the first measurement. (*H*) Photon counting distribution of a sample cell 3 h after DNA damage with binning of 1 μs.

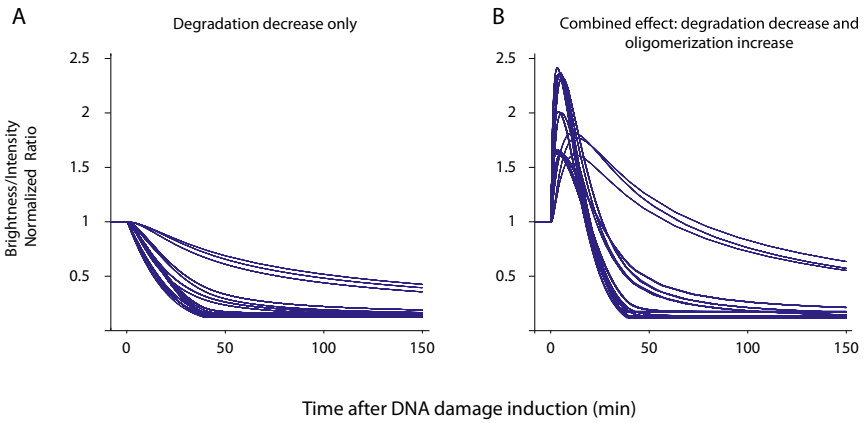

Fig. S3. The requirement for DNA to induce oligomerization directly is independent of the parameter set chosen. The model was run for all of the 349 parameter sets that match the experimental data at time 0. (*A*) If DNA damage is modeled only as a reduction in p53 protein degradation, the ratio of particle brightness over total intensity remains below 1 independently of the parameters chosen. Hence oligomeric p53 cannot increase more than the total intensity. (*B*) If DNA damage is modeled both as a reduction in p53 protein degradation and as an increase in p53 tetramerization, there is an initial window of time in which oligomeric p53 increases more than the total p53. This was the case for all of the parameter sets tested.

Table S1. Mathematical model equations presented in Fig. 3

$$\frac{dM}{dt} = a - 2\,k_{on}^{dim}\,M^2 + 2\;k_{off}^{dim}\;D - b_m\,M$$
$$\frac{dD}{dt} = +\,k_{on}^{dim}\;M^2 - k_{off}^{dim}\;D - 2\,k_{on}^{tet}\;D^2 + 2\,k_{off}^{tet}\;T - b_d\,D$$
$$\frac{dT}{dt} = +\,k_{on}^{tet}\,D^2 - k_{off}^{tet}\;T - b_t\,T$$

Ordinary differential equations used to model the dynamics of p53 oligomerization, from monomeric p53 (*M*) to dimeric (*D*) and tetrameric p53 (*T*). A full description of the parameters is given in Table S2.

Table S2. Parameters of the mathematical model presented in Fig. 3

Parameter	Description
a	Production rate of p53 molecules
k_{on}^{dim}	Dimerization reaction on-rate
k_{off}^{dim}	Dimerization reaction off-rate
k_{on}^{tet}	Tetramerization reaction on-rate
k_{off}^{tet}	Tetramerization reaction off-rate
b_m	Monomeric p53 degradation rate
b_d	Dimeric p53 degradation rate
b_t	Tetrameric p53 degradation rate

In the initial analysis all parameters were allowed to span a range of seven orders of magnitude. The choice of parameters is described in *Materials and Methods*.

Table S3. Experimentally tested parameters

Physical parameter	Description	Model parameter	Value	Source
K_d Mono-Dim	Dissociation constant of dimerization reaction	$k_{off}^{dim}/k_{on}^{dim}$	~0.55 nM	Rajagopalan et al. (1)
K_d Dim-Tet	Dissociation constant of tetramerization reaction	$k_{off}^{tet}/k_{on}^{tet}$	100 nM–1 μM	Rajagopalan et al. (2), Weinberg et al. (3)
t_{half} monomer	Half-life of monomeric p53	$1/b_m$	~1,000 min	Fig. 2

Table of biophysical experimental measurements and their corresponding model parameters.

1. Rajagopalan S, Huang F, Fersht AR (2011) Single-molecule characterization of oligomerization kinetics and equilibria of the tumor suppressor p53. *Nucleic Acids Res* 39(6):2294–2303.
2. Rajagopalan S, Jaulent AM, Wells M, Veprintsev DB, Fersht AR (2008) 14-3-3 activation of DNA binding of p53 by enhancing its association into tetramers. *Nucleic Acids Res* 36(18): 5983–5991.
3. Weinberg RL, Veprintsev DB, Fersht AR (2004) Cooperative binding of tetrameric p53 to DNA. *J Mol Biol* 341(5):1145–1159.